NANO LETTERS

pubs.acs.org/NanoLett

Letter

Nucleophilic Interfacial Layer Enables Stable Zn Anodes for Aqueous Zn Batteries

Yan Xu, Xinhua Zheng, Jifei Sun, Weiping Wang, Mingming Wang, Yuan Yuan, Mingyan Chuai, Na Chen, Hanlin Hu,* and Wei Chen*

Cite This: https://doi.org/10.1021/acs.nanolett.2c00398

Read Online

ACCESS | Metrics & More | Article Recommendations | Supporting Information

ABSTRACT: Aqueous Zn batteries are emerging as promising energy storage devices. However, severe dendrite growth and side reactions of Zn anodes restrict their further development. Herein, we develop a nucleophilic interfacial layer (NIL) on Zn to achieve a highly stable Zn anode for rechargeable Zn batteries. The NIL in a composition of zinc acetate acetamide is homogeneous, compact, and Zn^{2+}-conductive, rendering dendrite-free Zn deposition, which is observed by in situ optical microscopy. Benefiting from the advantages of NIL, the Zn||Zn symmetric cells show a low overpotential of 0.12 V at a high current density of 40 mA/cm^2, enhanced Coulombic efficiency up to 99.9%, and extended lifespan over 2600 cycles. The Zn||Ti asymmetric cells exhibit a high areal capacity of 5 mAh/cm^2. Moreover, the NIL functionalized Zn anode enables stable cycling of both anode-free Zn||Cl_2 cells and zinc-ion capacitors, providing opportunities for the development of high-performance energy storage devices.

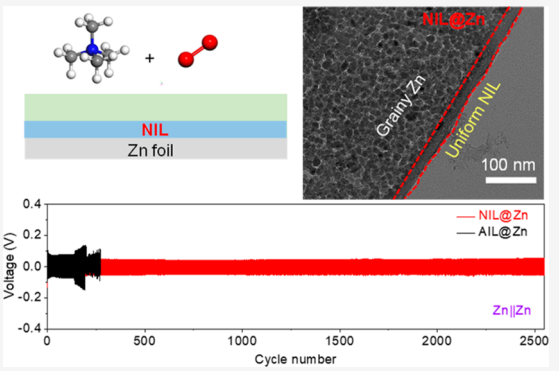

KEYWORDS: *Nucleophilic interfacial layer, nucleophilic agent, Zn anode, dendrite-free, Zn||Cl_2 battery, zinc ion capacitor*

Zinc batteries have emerged as a promising alternative to lithium-ion batteries because of their high volumetric capacity (5855 mAh/cm^3), environmental friendliness, and rich element abundance.[1−13] Aqueous Zn batteries could offer fast kinetics and high safety. However, the Zn anode suffers from dendrite growth due to the inhomogeneous distribution of $Zn(OH)_2$-based interfacial layer on Zn anode, which leads to low Coulombic efficiency (CE) of Zn batteries.[14−19] In addition, side reactions,[17,20−24] such as hydrogen evolution reaction (HER) and chemical corrosion, occur on the Zn surface, which exacerbate the failure of the Zn anode.

An effective method to suppress the dendrite growth and side reactions on metallic Zn is to construct a Zn^{2+}-conducting solid−electrolyte interface in aqueous electrolytes.[25−29] Previously, carbon-based materials,[30,31] metal nanoparticles,[32,33] inorganic compounds,[27−29] polymers,[25,34] and organic/inorganic composites[26,35] have been designed to coat on a Zn anode to improve its electrochemical properties. For instance, Li[36] et al. constructed a 3D ZnF_2 matrix on Zn anode by an electrochemical method, which extended the cycle life of Zn||Zn symmetric cells to 800 h at 1 mA/cm^2 with a capacity of 1 mAh/cm^2. Jang and Grzybowski[37] et al. produced thin covalent organic frameworks by self-assembly on Zn anode, which enabled cycling of Zn||Zn symmetric cells for 420 h at 1 mA/cm^2. Alshareef[38] et al. spin-coated selectively polarized ferroelectric polymer materials to a Zn anode, and the Zn||Zn symmetric cells exhibited a long cycling lifespan of 2000 h at 0.2 mA/cm^2 with a capacity of 0.2 mAh/cm^2. So far, although high performance Zn anode can be achieved, complicated preparation procedures are required for the fabrication of these interfacial layers. Therefore, convenient and effective approaches to fabricate interfacial layers for Zn anode are urgently required.

Nucleophilic agent is a reactant that forms bonds with its reactive partner of electrophilic agent by donating an electron pair, which can be initiated and accelerated by the presence of metal ions.[39,40] By applying this characteristic of nucleophilic agent, an interfacial layer can be constructed on Zn anode by a well-designed reaction path. Dissolved oxygen in the aqueous electrolyte can act as a natural electrophilic agent. Therefore, the key for the formation of such interfacial layers relies on the screening of nucleophilic agents with suitable electronic donation property. It is worth mentioning that to ensure redox reaction between the nucleophilic agents and oxidant, the decomposition reaction between metal anode and

Received: January 29, 2022
Revised: March 27, 2022

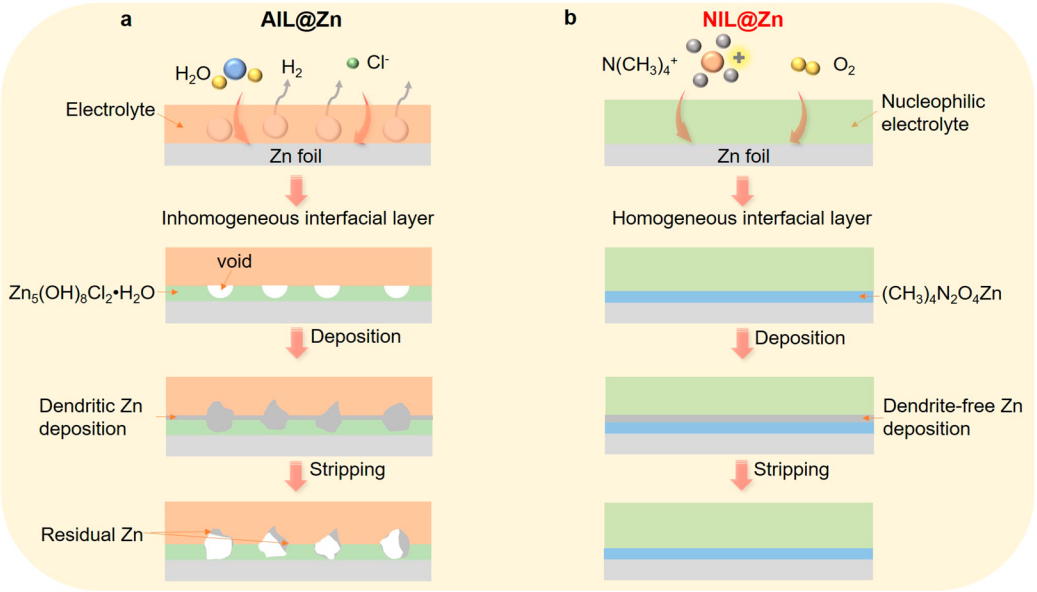

Figure 1. Schematic diagram of the formation of interfacial layers on Zn anode (a) in the control electrolyte of $ZnSO_4$−LiCl and (b) in the nucleophilic electrolyte of $ZnSO_4$−LiCl−TMACl.

nucleophilic agent should be prohibited. While in the traditional aqueous electrolyte, H_2O is a strong nucleophilic agent, which reacts directly and vigorously with Zn, the generated H_2 bubbles are detrimental to the homogeneous formation of interfacial layer, leading to inhomogeneous Zn^{2+} distribution and dendrite formation. On the basis of the above analysis, an ideal nucleophilic agent should have the following properties: (1) gas-free generation during reaction, which entails the homogeneity of the formed interfacial layer; (2) proper nucleophilicity, which can avoid its reaction with Zn directly and guarantee the reaction between nucleophilic agent and O_2. It is well-known that N-containing compounds have weaker nucleophilicity than O-containing compounds. In addition, N-containing solid−electrolyte interfaces have been verified to be effective to protect Li and Zn anodes.[41−43] Therefore, we propose in this study that N-containing nucleophilic agents can be applied to form interfacial layers to protect Zn anode.

In this study, we report highly stable Zn electrodes with a unique nucleophilic interfacial layer (NIL) for high-performance aqueous Zn metal batteries. We choose tetramethylammonium chloride (TMACl) as the N-containing nucleophilic agent due to its proper nucleophilic characteristics in the electrolyte of $ZnSO_4$. A uniform NIL of zinc acetate acetamide can be constructed due to its gas-free generation characteristic of the reaction between the nucleophilic agent and O_2, which is different from the inhomogeneous alkaline interfacial layer (AIL) of $Zn_5(OH)_8Cl_2{\cdot}H_2O$ in the control electrolyte of $ZnSO_4$. Benefiting from the homogeneity of the NIL, CE of Zn electroplating/stripping can be enhanced from 87.6% to 99.9%. Further, this in situ formed NIL renders the operation of Zn||Zn symmetric cells with over 2600 cycles at a capacity of 1 mAh/cm^2. In addition, the polarization of Zn||Zn symmetric cell is merely 0.12 V at a high current density of 40 mA/cm^2 due to the high conductivity of Zn^{2+} in the NIL. More importantly, the NIL-functionalized Zn (NIL@Zn) anode enables reversible operations with stable cycling of an anode-free Zn||Cl_2 cell and zinc ion capacitor for 200 and 60 000 cycles, respectively.

RESULTS AND DISCUSSION

The formation processes of NIL and AIL with their protective mechanisms during the Zn plating/stripping process are displayed in Figure 1a and b. In the aqueous electrolyte of $ZnSO_4$−LiCl, H_2O readily reacts with metallic Zn and generates H_2 gas, which results in the formation of $Zn(OH)_2$ with uneven thickness (Figure 1a). Because the radii of Cl^- anions are smaller than those of SO_4^{2-}, Cl^- anions are easier to combine with $Zn(OH)_2$ and finally form $Zn_5(OH)_8Cl_2{\cdot}H_2O$ inhomogeneous AIL on the surface of Zn anode. During the deposition process, Zn^{2+} ions are preferred to grow around thinner areas of the interfacial layers due to the low resistance, and eventually, dendritic morphology of deposited Zn can be observed. While in the nucleophilic electrolyte of $ZnSO_4$−LiCl−TMACl, Zn^{2+} ions promote the reaction kinetics between $N(CH_3)_4^+$ ions and O_2[44] (Figure 1b) and finally form a zinc acetate acetamide protective layer. The NIL kept in a good structure after many deposition/stripping cycles. The formation mechanism of NIL was described in detail in Figure S1.

To verify the reaction priority of H_2O and $N(CH_3)_4^+$ ions in the nucleophilic electrolyte, the ability to donate electron was expressed through molecular orbital level by DFT calculation. As shown in Figure 2a, $(CH_3)_4NCl$ has a higher position of the highest occupied molecular orbital (HOMO) than that of H_2O (−0.19213 eV vs −0.31926 eV); thus, $(CH_3)_4NCl$ is easier to donate electron than H_2O. X-ray diffraction (XRD) and X-ray photoelectron spectroscopy (XPS) characterizations were used to investigate the components of AIL and NIL. As shown in Figure 2b, XRD indicated that AIL@Zn anode showed a $Zn_5(OH)_8Cl_2{\cdot}H_2O$ composition, which is identical to previous reported literature.[45,46] In contrast, the NIL@Zn anode presented a distinct surface composition. A strong peak at 15.5° and small peaks at 30.3°, 31.1°, 42°, and 44.7° can be observed, corresponding to the formation of $C_4H_{10}N_2O_2{\cdot}Zn(CH_3COO)_2$, which is consistent with our hypothesis. It is worth noting that small XRD peaks ascribed to $Zn_2OCl_2{\cdot}2H_2O$ can be observed, which may be due to the attack of Cl^- ions to Zn anode. In addition, Zn, C, N, O, and Cl elements can be

https://doi.org/10.1021/acs.nanolett.2c00398
Nano Lett. XXXX, XXX, XXX−XXX

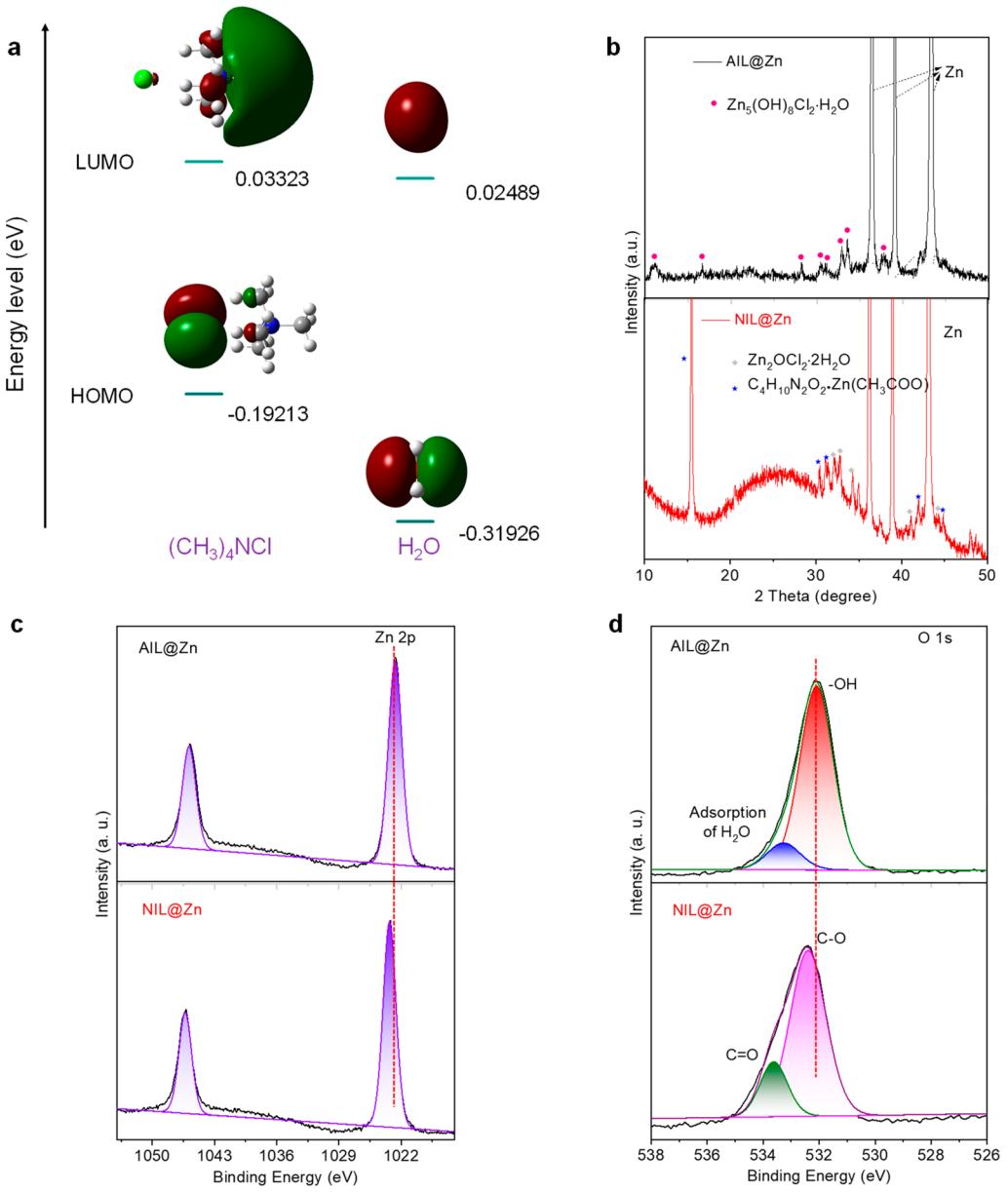

Figure 2. (a) LUMO, HOMO isosurfaces of $(CH_3)_4NCl$ (left) and H_2O molecules (right). (b) XRD of AIL@Zn and NIL@Zn. (c) Zn 2p and (d) O 1s XPS spectra of AIL@Zn and NIL@Zn.

detected by EDX mapping and showed uniform distribution on the NIL@Zn anode (Figure S2), which further confirm the formation of $C_4H_{10}N_2O_2{\cdot}Zn(CH_3COO)_2$ (PDF: #33−1977) and $Zn_2OCl_2{\cdot}2H_2O$ in the NIL. To verify the importance of O_2 in the nucleophilic reaction, the component of the cycled Zn anode in O_2-free nucleophilic electrolyte of $ZnSO_4$−LiCl−TMACl was tested. As shown in Figure S3, XRD peaks of the cycled Zn anode in O_2-free nucleophilic electrolyte are distinct from the Zn anode with NIL, which indicated the importance of O_2 for the nucleophilic reaction. In addition, the cycling life of Zn||Zn symmetric cells in the O_2-free nucleophilic electrolyte of $ZnSO_4$−LiCl−TMACl shrunk to 700 cycles (Figure S4), which indicated that the interfacial layer formed in the O_2-free nucleophilic electrolyte is not beneficial to the reversibility of Zn anode. XPS was further applied to verify the surface composition of AIL and NIL. In the AIL, the peak position of Zn 2p was located at 1022.6 eV, which can be ascribed to the $Zn_5(OH)_8Cl_2{\cdot}H_2O$ byproduct. Compared with the AIL of $Zn_5(OH)_8Cl_2{\cdot}H_2O$, the Zn 2p and O 1s XPS spectra of the NIL components showed 0.7 and 0.3 eV higher energy shifts to 1023.3 and 532.4 eV (Figure 2c,d), respectively, which indicated the different chemical environment of Zn^{2+} and O^{2-} in these two interfacial layers. Specifically, inorganic −OH group was detected at the binding energy of 532.0 eV by O 1s spectra in the AIL (Figure 2d), which can be ascribed to $Zn_5(OH)_8Cl_2{\cdot}H_2O$. While in the NIL, the O 1s signal can be deconvoluted into binding energies of 533.6 and 532.4 eV, which are ascribed to C=O and C−O groups that originate from the acetate and acetamide, respectively. These results further verified the formation mechanism of the NIL that was through the reaction between nucleophilic agent and O_2 for Zn anode.

Because the nucleophilic reaction process mildly proceeds without gas generation, the resulting NIL layer shows a uniform morphology. Therefore, much more nucleation sites can be offered for Zn^{2+} access, which guarantees the high

https://doi.org/10.1021/acs.nanolett.2c00398
Nano Lett. XXXX, XXX, XXX−XXX

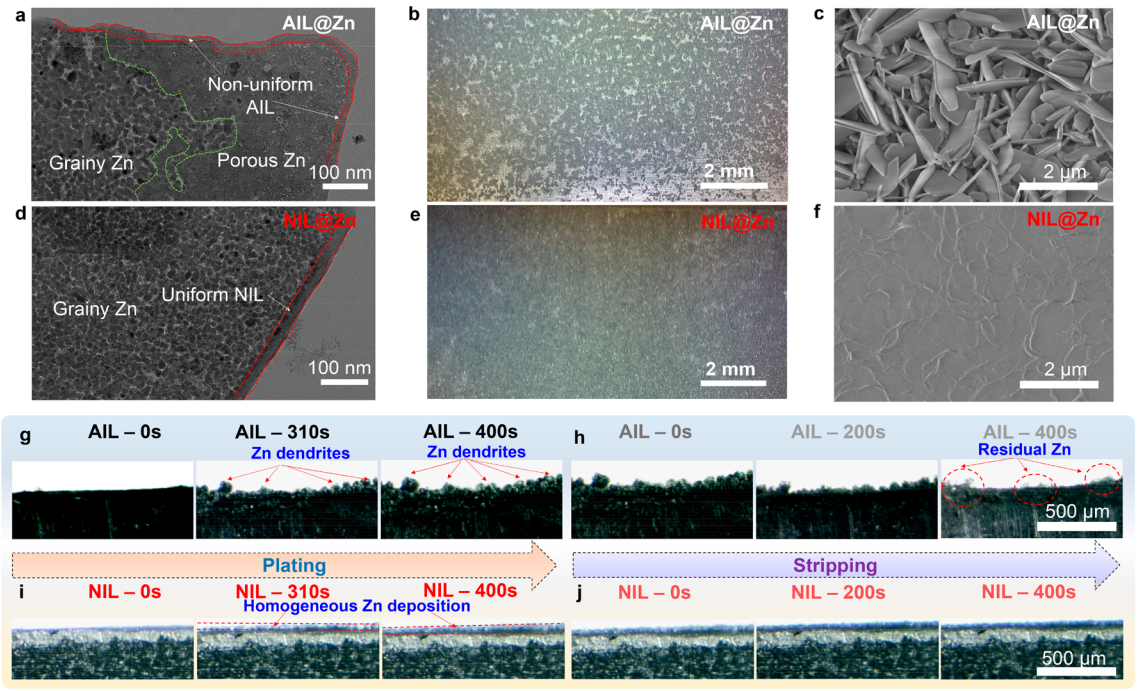

Figure 3. TEM images of the deposited Zn with (a) AIL and (d) NIL. Optical images of the deposited Zn with a capacity of 10 mAh/cm^2 on (b) AIL@Zn foil and (e) NIL@Zn foil substrates. The black part is the deposited Zn, and the silver part is the Zn foil substrate. SEM images of deposited Zn (c) with AIL and (f) with NIL. In situ optical microscopy images of the plating/stripping processes of Zn with AIL (g, h) and with NIL (i, j) at a current density of 10 mA/cm^2.

reversibility of Zn plating/stripping. Transmission electron microscopy (TEM) was applied to verify how H_2 generation affect the uniformity of the interfacial layers in both electrolytes. As shown in Figure 3a and b, triggered by the H_2 generation, the thickness of AIL is in a wide range of 5−20 nm (Figure 3a) in the control electrolyte, which results in the distinct penetration of Zn^{2+} in different areas. Therefore, the deposited Zn in Figure 3a shows morphologies of grainy and porous structures in different areas. In contrast, the NIL is highly uniform with a thickness of ∼15 nm (Figure 3d). With the benefits of uniform NIL, only grainy structure can be observed in Figure 3d. Further, the uniformity of the interfacial layers was verified in large scale by optical microscopy. An areal capacity of 10 mAh/cm^2 of Zn was deposited on Zn foil substrate and then characterized by the optical microscopy. As shown in Figure 3b and e, the deposited Zn with AIL is discrete. However, the deposited Zn with NIL is uniformly distributed, which further verified the homogeneous distribution of the NIL. Scanning electron microscopy (SEM) was further applied to study how AIL and NIL affect the nucleation and growth process of Zn. Dendritic Zn surface can be obviously observed on the cycled Zn anode with AIL (Figure 3c), which implied that the deposited Zn continued to grow on the Zn seeds due to the rare and ununiformed nucleation sites, resulting in the dendritic morphology. Because of the rich nucleation sites in the protective layer of NIL, the deposited Zn became uniform (Figure 3f). This feature is important for the electrodeposition/stripping of Zn in the battery operation conditions.

Moreover, an in situ optical microscope was used to monitor the surface morphology evolution during the Zn plating/stripping processes. The homemade glass cell for in situ optical microscopy test was shown in Figure S5. As shown in Figure 3g, mossy Zn can be observed on the substrate of AIL@Zn after Zn plating, and residual Zn can be observed on AIL@Zn after fully stripping even within only one cycle (Figure 3h and Supporting Video 1). In sharp contrast, a homogeneous and uniform Zn deposition process can be observed on the substrate of NIL@Zn (Figure 3i), indicating the homogeneous and dendrite-free growth of Zn with the NIL. More importantly, no "dead" Zn can be observed after fully stripping (Figure 3j and Supporting Video 2), which indicates the high reversibility of Zn with NIL.

Zn Plating/Stripping Reversibility. To verify the protective effect of NIL and AIL, asymmetric Zn||Ti cells were assembled in the conditions of AIL@Zn and NIL@Zn anodes, separately (Figure 4a,b). Zn plating/stripping on the Ti substrate showed comparable overpotentials of ∼30 mV with AIL and NIL due to their comparable interfacial resistance. However, the Zn plating/stripping efficiency was improved from 97.5% to 99.6% at a current density of 10 mA/cm^2 with an areal capacity of 5 mAh/cm^2 in the presence of NIL (Figure 4c). The higher intactness of the interfacial layer, the better resistance it will have to water corrosion. To further explore the suppression of side reactions on AIL@Zn and NIL@Zn anodes, linear sweep voltammetry (LSV) and Tafel plot were recorded using Zn||Ti cells and Zn−Ag/AgCl-Pt cells in the Na_2SO_4 solution. As shown in Figure S6, the overpotential of HER increased about 20 mV on NIL@Zn, and the HER current density of NIL@Zn was lower than that of AIL@Zn. In addition, the corrosion current density of NIL@Zn was 0.16 μA/cm^2 lower than AIL@Zn (Figure S7). All of these results verified that the NIL is more intact and homogeneous than the AIL against hydrogen evolution and chemical corrosion, which guaranteed the high stability of Zn battery.

Zn||Zn symmetric cells were further assembled to verify the role of the interfacial layers in improving the electrochemical

https://doi.org/10.1021/acs.nanolett.2c00398
Nano Lett. XXXX, XXX, XXX−XXX

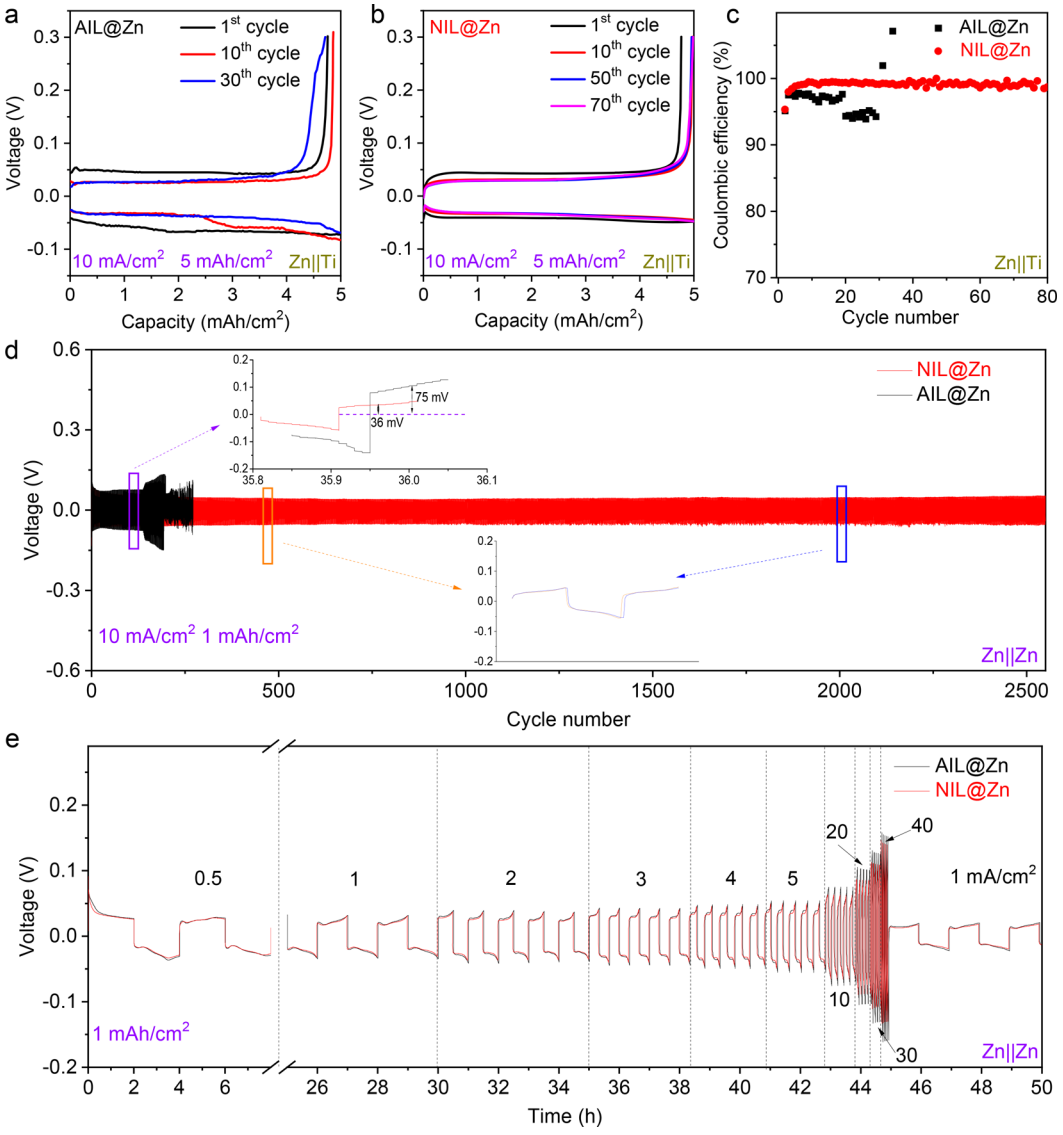

Figure 4. Electrochemical performance of the Zn||Zn symmetric cells and Zn||Ti asymmetric cells. Voltage profiles of Zn||Ti cells (a) with AIL and (b) with NIL. (c) Coulombic efficiency of Zn||Ti cells with AIL and with NIL. (d) Time−voltage profiles of AIL@Zn||AIL@Zn and NIL@Zn||NIL@Zn symmetric cells at a current density of 10 mA/cm^2 with an areal capacity of 1 mAh/cm^2. (e) Rate capability profiles of AIL@Zn||AIL@Zn and NIL@Zn||NIL@Zn symmetric cells at various current densities with a capacity of 1 mAh/cm^2.

performance of Zn electrode. Figure 4d showed the typical voltage profile of the AIL@Zn||AIL@Zn and NIL@Zn||NIL@Zn symmetric cells, where the AIL@Zn||AIL@Zn cell exhibited stable Zn stripping/plating cycling with an average overpotential of ∼150 mV for the initial 140 cycles at 10 mA/cm^2 and 1 mAh/cm^2. The overpotential gradually increased over further cycling and reached ∼270 mV at the 200th cycle, and eventually the AIL@Zn||AIL@Zn cell failed after only 200 cycles due to the short circuit of Zn dendrites. In sharp contrast, the NIL@Zn||NIL@Zn symmetric cell exhibited stable Zn plating/stripping cycling for over 2600 cycles with an average overpotential of ∼72 mV, demonstrating the important role of homogeneous NIL in improving the electrochemical reversibility of Zn electrode. Remarkably, at a high current density of 40 mA/cm^2 with an areal capacity of 1 mAh/cm^2, stable Zn plating/stripping cycling with an average overpotential of 120 mV for more than 2800 cycles was achieved for the NIL@Zn||NIL@Zn symmetric cell (Figure S8). As a comparison, the AIL@Zn||AIL@Zn symmetric cell failed within 200 cycles under the same conditions. We conducted comparation of our work with recently reported work in Figure S9. Encouragingly, our work exhibits an impressive current density (10 mA/cm^2) with long cycle life, demonstrating the outstanding effect of the NIL on protecting Zn anode.

Ionic conductivity of the AIL and NIL was evaluated by electrochemical impedance spectroscopy (EIS) in the Zn||Zn symmetric cells. As shown in Figure S10, the interfacial impedance of the NIL@Zn anode was smaller than that of the AIL@Zn, suggesting a better Zn^{2+} conductivity of the NIL. The Zn^{2+} conductivity was further investigated by the Zn||Zn symmetric cells under various current densities from 0.5 mA/cm^2 to 40 mA/cm^2. As shown in Figures 4e and S11, the polarization voltages of the AIL@Zn||AIL@Zn and NIL@Zn||NIL@Zn symmetric cells were comparable under low current densities (0.5 mA/cm^2 and 1 mA/cm^2). However, with the current density increases (10 to 40 mA/cm^2), the NIL@Zn||NIL@Zn symmetric cell exhibited substantially lower overpotentials than that of the AIL@Zn||AIL@Zn symmetric cell,

https://doi.org/10.1021/acs.nanolett.2c00398
Nano Lett. XXXX, XXX, XXX−XXX

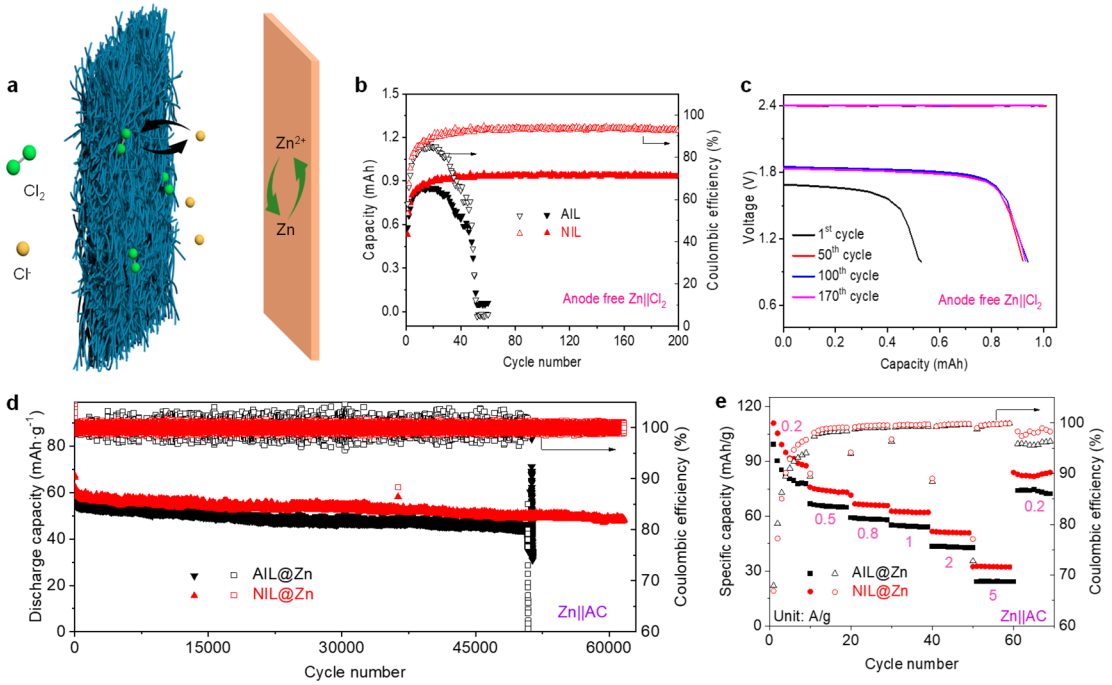

Figure 5. Electrochemical performance of NIL@Zn-based energy storage systems in full cells. (a) Schematic diagram of Zn||Cl_2 battery. (b) Cycling performance of anode-free Zn||Cl_2 cell with AIL and NIL. (c) Voltage profiles of anode-free Zn||Cl_2 cell with NIL at different cycles. (d) Cycling performances of zinc ion capacitors with AIL and NIL at 1 A/g. (e) Rate capability of zinc ion capacitors with AIL and NIL at different current densities.

which indicated the favorable Zn^{2+} transportation in the NIL. The contact angles of AIL and NIL with electrolytes were measured to be 85.8° and 90.6°, respectively, which indicated that the AIL and NIL did not change much on the affinity of the electrolytes with the Zn anode (Figure S12).

To verify the feasibility of the NIL, we have fabricated Zn||Cl_2 cells by applying the NIL@Zn foil as the anode and Cl_2 as the cathode. It was reported that Cl_2 has a high theoretical volumetric energy density (2500 Wh/L) and abundant elemental availability. Therefore, aqueous Zn||Cl_2 battery chemistry has received much attention since the 1980s due to its conceptually simple redox reaction ($Zn + Cl_2 \leftrightarrow ZnCl_2$) and cheap materials for fabrication.

The schematic diagram of Zn||Cl_2 cells is shown in Figure 5a. When charging the Zn||Cl_2 cells, LiCl solution in the electrolyte is electrolyzed to generate Cl_2 on the cathode porous carbon felt; meanwhile, Zn is plated on the anode. During discharge of the battery, the Cl_2 on the carbon felt is reduced back to soluble Cl^-, and Zn is stripped from the Zn anode. As shown in Figure S13, both the CV curves of the NIL@Zn||Cl_2 and AIL@Zn||Cl_2 cells at 5 mV/s showed similar redox behaviors, which exhibited one pair of oxidation and reduction peaks, corresponding to the Cl^-/Cl_2 reactions on the cathode and the Zn/Zn^{2+} reactions on the anode. It should be noted that in the absence of NIL, the redox current densities of the AIL@Zn were lower and the discharge plateau was 0.04 V lower than that of the NIL@Zn, suggesting that the NIL was also favorable for the charge transfer. In addition, we fabricated a Zn||Cl_2 cell in an anode-free configuration, which is considered to be very challenging for the Zn metal batteries. As shown in Figure 5b, the cycling performance and corresponding CEs of the anode-free Zn||Cl_2 cells with AIL and NIL were tested at 20 mA/cm^2. An activation process was needed in the initial cycles for the cells with AIL and NIL. The CE only reached 85% for the anode-free AIL@Zn||Cl_2 cell, which failed within 50 cycles. In contrast, the CE of the anode-free NIL@Zn||Cl_2 cell can go up to 95% for over 200 cycles, which highlights the important role of the NIL for the high reversibility of Zn plating/stripping. The voltage profiles of the anode-free NIL@Zn||Cl_2 cell at different cycles were presented in Figure 5c. The discharge plateau reached 1.84 V and the discharge capacity remained at 0.95 mAh after the initial activation. It is important to point out that the Zn||Cl_2 battery chemistry presented in this study was only used to demonstrate the function of the NIL on the Zn anode. However, some critical issues regarding the Cl_2 cathode were not intended to be addressed, which are not the focus of the current work.

Furthermore, zinc ion capacitors were assembled by using the NIL@Zn anode and commercial porous carbon, showing a stable operation over 60 000 cycles at a current density of 1 A/g. In contrast, the zinc ion capacitor using the AIL@Zn anode confronted cell failure around 51 000 cycles (Figure 5d). The rate performance of the Zn ion capacitor with AIL and NIL was also investigated, as shown in Figure 5e. In the NIL@Zn ion capacitor, high capacities of 88, 76, 67, 63, 51, and 33 mAh/g could be achieved at 0.2, 0.5, 0.8, 1, 2, and 5 A g^{-1}, respectively. Notably, when the rate shifted gradually back to 0.2 A g^{-1} after the high-rate cycling, the highly reversible capacity recovered to 82 mAh/g, while the AIL@Zn ion capacitor showed a much lower capacity under the same current density, suggesting the effectiveness of the NIL in Zn ion capacitor.

In conclusion, a nucleophilic interfacial layer was constructed on Zn anode by introducing a nucleophilic agent, TMACl, into the electrolyte. The NIL was verified to be zinc acetate acetamide, which was drastically different from the AIL of $Zn_5(OH)_8Cl_2{\cdot}H_2O$ in the control electrolyte. On the basis

https://doi.org/10.1021/acs.nanolett.2c00398
Nano Lett. XXXX, XXX, XXX−XXX

of different characterizations including in situ optical microscopy, SEM, TEM, XRD, and XPS, we have demonstrated that the NIL is compact, homogeneous, and Zn^{2+}-conductive, which could effectively modulate the dendrite-free Zn deposition. The cycle life of the NIL@Zn||NIL@Zn symmetric cell was extended over 2600 cycles at a current density of 10 mA/cm^2 with an areal capacity of 1 mAh/cm^2, much superior to the AIL@Zn||AIL@Zn cell with only 200 cycles. Meanwhile, the Coulombic efficiency of Zn plating/stripping reactions was enhanced from 87.6% with the AIL@Zn anode to 99.9% with the NIL@Zn anode. In addition, the NIL@Zn anode enabled stable cycling of the Zn||Zn symmetric cell for over 2800 cycles at a high current density of 40 mA/cm^2 with a low overpotential of 0.12 V. Furthermore, the NIL-functionalized Zn anode enabled anode-free Zn||Cl_2 cell and zinc ion capacitor with improved electrochemical performances and long-term cycling stability. The design of nucleophilic interfacial layer on Zn anode may open up a new avenue for the exploration of effective metal anodes for high-performance metal batteries.

■ ASSOCIATED CONTENT

Supporting Information

The Supporting Information is available free of charge at https://pubs.acs.org/doi/10.1021/acs.nanolett.2c00398.

Experimental details, characterizations, DFT calculation, and supplementary figures (PDF)

Video 1 Zn plating/stripping of AIL@Zn. Two-electrode (Zn foil and Zn foil) configuration was applied for the in situ optical microscopy test in the electrolyte of 1 M $ZnSO_4$ − 1 M LiCl. The cell was placed at the specimen stage and the Zn foil was located perpendicular to the incident light source. Meanwhile, galvanostatic deposition was performed by an electrochemical workstation (CHI660E) under a current density of 10 mA/cm^2. (MP4)

SVideo 2 Zn plating/stripping of NIL@Zn. Two-electrode (Zn foil and Zn foil) configuration was applied for the in situ optical microscopy test in the electrolyte of 1 M $ZnSO_4$ − 1 M LiCl - 0.4 M TMACl. The cell was placed at the specimen stage and the Zn foil was located perpendicular to the incident light source. Meanwhile, galvanostatic deposition was performed by an electrochemical workstation (CHI660E) under a current density of 10 mA/cm^2. (MP4)

■ AUTHOR INFORMATION

Corresponding Authors

Wei Chen − *Department of Applied Chemistry, School of Chemistry and Materials Science, Hefei National Laboratory for Physical Sciences at the Microscale, University of Science and Technology of China, Hefei, Anhui 230026, China;* orcid.org/0000-0002-8018-4529; Email: weichen1@ustc.edu.cn

Hanlin Hu − *Hoffman Institute of Advanced Materials, Shenzhen Polytechnic, Shenzhen, Guangdong 518000, China;* Email: hanlinhu@szpt.edu.cn

Authors

Yan Xu − *Hoffman Institute of Advanced Materials, Shenzhen Polytechnic, Shenzhen, Guangdong 518000, China; Department of Applied Chemistry, School of Chemistry and Materials Science, Hefei National Laboratory for Physical Sciences at the Microscale, University of Science and Technology of China, Hefei, Anhui 230026, China*

Xinhua Zheng − *Department of Applied Chemistry, School of Chemistry and Materials Science, Hefei National Laboratory for Physical Sciences at the Microscale, University of Science and Technology of China, Hefei, Anhui 230026, China*

Jifei Sun − *Hoffman Institute of Advanced Materials, Shenzhen Polytechnic, Shenzhen, Guangdong 518000, China; Department of Applied Chemistry, School of Chemistry and Materials Science, Hefei National Laboratory for Physical Sciences at the Microscale, University of Science and Technology of China, Hefei, Anhui 230026, China*

Weiping Wang − *Department of Applied Chemistry, School of Chemistry and Materials Science, Hefei National Laboratory for Physical Sciences at the Microscale, University of Science and Technology of China, Hefei, Anhui 230026, China*

Mingming Wang − *Department of Applied Chemistry, School of Chemistry and Materials Science, Hefei National Laboratory for Physical Sciences at the Microscale, University of Science and Technology of China, Hefei, Anhui 230026, China*

Yuan Yuan − *Department of Applied Chemistry, School of Chemistry and Materials Science, Hefei National Laboratory for Physical Sciences at the Microscale, University of Science and Technology of China, Hefei, Anhui 230026, China*

Mingyan Chuai − *Department of Applied Chemistry, School of Chemistry and Materials Science, Hefei National Laboratory for Physical Sciences at the Microscale, University of Science and Technology of China, Hefei, Anhui 230026, China*

Na Chen − *Department of Applied Chemistry, School of Chemistry and Materials Science, Hefei National Laboratory for Physical Sciences at the Microscale, University of Science and Technology of China, Hefei, Anhui 230026, China*

Complete contact information is available at: https://pubs.acs.org/10.1021/acs.nanolett.2c00398

Notes

The authors declare no competing financial interest.

■ ACKNOWLEDGMENTS

This work was supported by the startup funds from USTC (Grant No. KY2060000150) and China Postdoctoral Science Foundation (2021M693061). We acknowledge the support from USTC Center for Micro and Nanoscale Research and the advanced computing resources provided by the Supercomputing Center of the USTC.

■ REFERENCES

(1) Xu, K. Electrolytes and Interphases in Li-Ion Batteries and Beyond. *Chem. Rev.* **2014**, *114* (23), 11503−11618.

(2) Tikekar, M. D.; Choudhury, S.; Tu, Z.; Archer, L. A. Design principles for electrolytes and interfaces for stable lithium-metal batteries. *Nature Energy* **2016**, *1* (9), 16114.

(3) Tarascon, J. M.; Armand, M. Issues and challenges facing rechargeable lithium batteries. *Nature* **2001**, *414* (6861), 359−367.

(4) Zheng, J.; Zhao, Q.; Tang, T.; Yin, J.; Quilty, C. D.; Renderos, G. D.; Liu, X.; Deng, Y.; Wang, L.; Bock, D. C.; Jaye, C.; Zhang, D.; Takeuchi, E. S.; Takeuchi, K. J.; Marschilok, A. C.; Archer, L. A. Reversible epitaxial electrodeposition of metals in battery anodes. *Science* **2019**, *366* (6465), 645−648.

(5) Liang, X.; Pang, Q.; Kochetkov, I. R.; Sempere, M. S.; Huang, H.; Sun, X.; Nazar, L. F. A facile surface chemistry route to a stabilized lithium metal anode. *Nature Energy* **2017**, *2* (9), 17119.

(6) Wang, F.; Borodin, O.; Gao, T.; Fan, X.; Sun, W.; Han, F.; Faraone, A.; Dura, J. A.; Xu, K.; Wang, C. Highly reversible zinc metal anode for aqueous batteries. *Nat. Mater.* **2018**, *17* (6), 543−549.
(7) Parker, J. F.; Chervin, C. N.; Pala, I. R.; Machler, M.; Burz, M. F.; Long, J. W.; Rolison, D. R. Rechargeable nickel 3D zinc batteries: An energy-dense, safer alternative to lithium-ion. *Science* **2017**, *356* (6336), 415−418.
(8) Han, D.; Wang, Z.; Lu, H.; Li, H.; Cui, C.; Zhang, Z.; Sun, R.; Geng, C.; Liang, Q.; Guo, X.; Mo, Y.; Zhi, X.; Kang, F.; Weng, Z.; Yang, Q.-H. A Self-Regulated Interface toward Highly Reversible Aqueous Zinc Batteries. *Adv. Energy Mater.* **2022**, *12* (9), 2102982.
(9) Guan, K.; Tao, L.; Yang, R.; Zhang, H.; Wang, N.; Wan, H.; Cui, J.; Zhang, J.; Wang, H.; Wang, H. Anti-Corrosion for Reversible Zinc Anode via a Hydrophobic Interface in Aqueous Zinc Batteries. *Adv. Energy Mater.* **2022**, *12* (9), 2103557.
(10) Sun, P.; Ma, L.; Zhou, W.; Qiu, M.; Wang, Z.; Chao, D.; Mai, W. Simultaneous Regulation on Solvation Shell and Electrode Interface for Dendrite-Free Zn Ion Batteries Achieved by a Low-Cost Glucose Additive. *Angew. Chem., Int. Ed.* **2021**, *60* (33), 18247−18255.
(11) Zeng, X.; Mao, J.; Hao, J.; Liu, J.; Liu, S.; Wang, Z.; Wang, Y.; Zhang, S.; Zheng, T.; Liu, J.; Rao, P.; Guo, Z. Electrolyte Design for In Situ Construction of Highly Zn^{2+}-Conductive Solid Electrolyte Interphase to Enable High-Performance Aqueous Zn-Ion Batteries under Practical Conditions. *Adv. Mater.* **2021**, *33* (11), 2007416.
(12) Qian, L.; Yao, W.; Yao, R.; Sui, Y.; Zhu, H.; Wang, F.; Zhao, J.; Zhi, C.; Yang, C. Cations Coordination-Regulated Reversibility Enhancement for Aqueous Zn-Ion Battery. *Adv. Funct. Mater.* **2021**, *31* (40), 2105736.
(13) Lu, H.; Zhang, X.; Luo, M.; Cao, K.; Lu, Y.; Xu, B. B.; Pan, H.; Tao, K.; Jiang, Y. Amino Acid-Induced Interface Charge Engineering Enables Highly Reversible Zn Anode. *Adv. Funct. Mater.* **2021**, *31* (45), 2103514.
(14) Cao, L.; Li, D.; Deng, T.; Li, Q.; Wang, C. Hydrophobic Organic-Electrolyte-Protected Zinc Anodes for Aqueous Zinc Batteries. *Angew. Chem., Int. Ed.* **2020**, *59* (43), 19292−19296.
(15) Cai, Z.; Ou, Y.; Zhang, B.; Wang, J.; Fu, L.; Wan, M.; Li, G.; Wang, W.; Wang, L.; Jiang, J.; Seh, Z. W.; Hu, E.; Yang, X.-Q.; Cui, Y.; Sun, Y. A Replacement Reaction Enabled Interdigitated Metal/Solid Electrolyte Architecture for Battery Cycling at 20 mA cm^{-2} and 20 mAh cm^{-2}. *J. Am. Chem. Soc.* **2021**, *143* (8), 3143−3152.
(16) Cao, L.; Li, D.; Pollard, T.; Deng, T.; Zhang, B.; Yang, C.; Chen, L.; Vatamanu, J.; Hu, E.; Hourwitz, M. J.; Ma, L.; Ding, M.; Li, Q.; Hou, S.; Gaskell, K.; Fourkas, J. T.; Yang, X.-Q.; Xu, K.; Borodin, O.; Wang, C. Fluorinated interphase enables reversible aqueous zinc battery chemistries. *Nat. Nanotechnol.* **2021**, *16* (8), 902−910.
(17) Cao, J.; Zhang, D.; Gu, C.; Wang, X.; Wang, S.; Zhang, X.; Qin, J.; Wu, Z.-S. Manipulating Crystallographic Orientation of Zinc Deposition for Dendrite-free Zinc Ion Batteries. *Adv. Energy Mater.* **2021**, *11* (29), 2101299.
(18) Du, W.; Ang, E. H.; Yang, Y.; Zhang, Y.; Ye, M.; Li, C. C. Challenges in the material and structural design of zinc anode towards high-performance aqueous zinc-ion batteries. *Energy Environ. Sci.* **2020**, *13* (10), 3330−3360.
(19) Cao, Z.; Zhuang, P.; Zhang, X.; Ye, M.; Shen, J.; Ajayan, P. M. Strategies for Dendrite-Free Anode in Aqueous Rechargeable Zinc Ion Batteries. *Adv. Energy Mater.* **2020**, *10* (30), 2001599.
(20) Wang, Y.; Guo, T.; Yin, J.; Tian, Z.; Ma, Y.; Liu, Z.; Zhu, Y.; Alshareef, H. N. Controlled Deposition of Zinc Metal Anodes via Selectively Polarized Ferroelectric Polymers. *Adv. Mater.* **2022**, *34*, 2106937.
(21) Wang, M.; Zheng, X.; Zhang, X.; Chao, D.; Qiao, S.-Z.; Alshareef, H. N.; Cui, Y.; Chen, W. Opportunities of Aqueous Manganese-Based Batteries with Deposition and Stripping Chemistry. *Adv. Energy Mater.* **2021**, *11* (5), 2002904.
(22) Liang, G.; Zhu, J.; Yan, B.; Li, Q.; Chen, A.; Chen, Z.; Wang, X.; Xiong, B.; Fan, J.; Xu, J.; Zhi, C. Gradient fluorinated alloy to enable highly reversible Zn-metal anode chemistry. *Energ Environ. Sci.* **2022**, *15*, 1086−1096.
(23) Zheng, X.; Ahmad, T.; Chen, W. Challenges and strategies on Zn electrodeposition for stable Zn-ion batteries. *Energy Storage Mater.* **2021**, *39*, 365−394.
(24) Yang, Q.; Li, L.; Hussain, T.; Wang, D.; Hui, L.; Guo, Y.; Liang, G.; Li, X.; Chen, Z.; Huang, Z.; Li, Y.; Xue, Y.; Zuo, Z.; Qiu, J.; Li, Y.; Zhi, C. Stabilizing Interface pH by N-Modified Graphdiyne for Dendrite-Free and High-Rate Aqueous Zn-Ion Batteries. *Angew. Chem., Int. Ed.* **2022**, *61* (6), No. e202112304.
(25) Zhao, Z.; Zhao, J.; Hu, Z.; Li, J.; Li, J.; Zhang, Y.; Wang, C.; Cui, G. Long-life and deeply rechargeable aqueous Zn anodes enabled by a multifunctional brightener-inspired interphase. *Energ Environ. Sci.* **2019**, *12* (6), 1938−1949.
(26) Cui, Y.; Zhao, Q.; Wu, X.; Chen, X.; Yang, J.; Wang, Y.; Qin, R.; Ding, S.; Song, Y.; Wu, J.; Yang, K.; Wang, Z.; Mei, Z.; Song, Z.; Wu, H.; Jiang, Z.; Qian, G.; Yang, L.; Pan, F. An Interface-Bridged Organic−Inorganic Layer that Suppresses Dendrite Formation and Side Reactions for Ultra-Long-Life Aqueous Zinc Metal Anodes. *Angew. Chem., Int. Ed.* **2020**, *59* (38), 16594−16601.
(27) Kang, L.; Cui, M.; Jiang, F.; Gao, Y.; Luo, H.; Liu, J.; Liang, W.; Zhi, C. Nanoporous $CaCO_3$ Coatings Enabled Uniform Zn Stripping/Plating for Long-Life Zinc Rechargeable Aqueous Batteries. *Adv. Energy Mater.* **2018**, *8* (25), 1801090.
(28) Zhao, K.; Wang, C.; Yu, Y.; Yan, M.; Wei, Q.; He, P.; Dong, Y.; Zhang, Z.; Wang, X.; Mai, L. Ultrathin Surface Coating Enables Stabilized Zinc Metal Anode. *Advanced Materials Interfaces* **2018**, *5* (16), 1800848.
(29) Zhang, Q.; Luan, J.; Huang, X.; Wang, Q.; Sun, D.; Tang, Y.; Ji, X.; Wang, H. Revealing the role of crystal orientation of protective layers for stable zinc anode. *Nat. Commun.* **2020**, *11* (1), 3961.
(30) Li, W.; Wang, K.; Zhou, M.; Zhan, H.; Cheng, S.; Jiang, K. Advanced Low-Cost, High-Voltage, Long-Life Aqueous Hybrid Sodium/Zinc Batteries Enabled by a Dendrite-Free Zinc Anode and Concentrated Electrolyte. *ACS Appl. Mater. Interfaces* **2018**, *10* (26), 22059−22066.
(31) Zeng, Y.; Zhang, X.; Qin, R.; Liu, X.; Fang, P.; Zheng, D.; Tong, Y.; Lu, X. Dendrite-Free Zinc Deposition Induced by Multifunctional CNT Frameworks for Stable Flexible Zn-Ion Batteries. *Adv. Mater.* **2019**, *31* (36), 1903675.
(32) Cui, M.; Xiao, Y.; Kang, L.; Du, W.; Gao, Y.; Sun, X.; Zhou, Y.; Li, X.; Li, H.; Jiang, F.; Zhi, C. Quasi-Isolated Au Particles as Heterogeneous Seeds To Guide Uniform Zn Deposition for Aqueous Zinc-Ion Batteries. *Acs. Appl. Energy Mater.* **2019**, *2* (9), 6490−6496.
(33) Yin, Y.; Wang, S.; Zhang, Q.; Song, Y.; Chang, N.; Pan, Y.; Zhang, H.; Li, X. Dendrite-Free Zinc Deposition Induced by Tin-Modified Multifunctional 3D Host for Stable Zinc-Based Flow Battery. *Adv. Mater.* **2020**, *32* (6), 1906803.
(34) Hieu, L. T.; So, S.; Kim, I. T.; Hur, J. Zn anode with flexible β-PVDF coating for aqueous Zn-ion batteries with long cycle life. *Chem. Eng. J.* **2021**, *411*, 128584.
(35) Yang, H.; Chang, Z.; Qiao, Y.; Deng, H.; Mu, X.; He, P.; Zhou, H. Constructing a Super-Saturated Electrolyte Front Surface for Stable Rechargeable Aqueous Zinc Batteries. *Angew. Chem., Int. Ed.* **2020**, *59* (24), 9377−9381.
(36) Yang, Y.; Liu, C.; Lv, Z.; Yang, H.; Zhang, Y.; Ye, M.; Chen, L.; Zhao, J.; Li, C. C. Synergistic Manipulation of Zn^{2+} Ion Flux and Desolvation Effect Enabled by Anodic Growth of a 3D ZnF_2 Matrix for Long-Lifespan and Dendrite-Free Zn Metal Anodes. *Adv. Mater.* **2021**, *33* (11), 2007388.
(37) Park, J. H.; Kwak, M.-J.; Hwang, C.; Kang, K.-N.; Liu, N.; Jang, J.-H.; Grzybowski, B. A. Self-Assembling Films of Covalent Organic Frameworks Enable Long-Term, Efficient Cycling of Zinc-Ion Batteries. *Adv. Mater.* **2021**, *33* (34), 2101726.
(38) Wang, Y.; Guo, T.; Yin, J.; Tian, Z.; Ma, Y.; Liu, Z.; Zhu, Y.; Alshareef, H. N. Controlled Deposition of Zinc-Metal Anodes via Selectively Polarized Ferroelectric Polymers. *Adv. Mater.* **2022**, *34*, 2106937.
(39) Fredriksen, S. B.; Jens, K.-J. Oxidative Degradation of Aqueous Amine Solutions of MEA, AMP, MDEA, Pz: A Review. *Energy Procedia* **2013**, *37*, 1770−1777.

https://doi.org/10.1021/acs.nanolett.2c00398
Nano Lett. XXXX, XXX, XXX−XXX

(40) Chi, S.; Rochelle, G. T. Oxidative Degradation of Monoethanolamine. *Ind. Eng. Chem. Res.* **2002**, *41* (17), 4178−4186.
(41) Bayer, M.; Overhoff, G. M.; Gui, A. L.; Winter, M.; Bieker, P.; Schulze, S. Influence of Water Content on the Surface Morphology of Zinc Deposited from EMImOTf/Water Mixtures. *J. Electrochem. Soc.* **2019**, *166* (6), A909−A914.
(42) Markevich, E.; Sharabi, R.; Borgel, V.; Gottlieb, H.; Salitra, G.; Aurbach, D.; Semrau, G.; Schmidt, M. A. In situ FTIR study of the decomposition of N-butyl-N-methylpyrrolidinium bis-(trifluoromethanesulfonyl)amide ionic liquid during cathodic polarization of lithium and graphite electrodes. *Electrochim. Acta* **2010**, *55* (8), 2687−2696.
(43) Preibisch, Y.; Horsthemke, F.; Winter, M.; Nowak, S.; Best, A. S. Is the Cation Innocent? An Analytical Approach on the Cationic Decomposition Behavior of N-Butyl-N-methylpyrrolidinium Bis-(trifluoromethanesulfonyl)imide in Contact with Lithium Metal. *Chem. Mater.* **2020**, *32* (6), 2389−2398.
(44) Pan, W.; Mao, J.; Wang, Y.; Zhao, X.; Leong, K. W.; Luo, S.; Chen, Y.; Leung, D. Y. C. High-Performance MnO_2/Al Battery with In Situ Electrochemically Reformed Al_xMnO_2 Nanosphere Cathode. *Small Methods* **2021**, *5*, 2100491.
(45) Cao, L.; Li, D.; Soto, F. A.; Ponce, V.; Zhang, B.; Ma, L.; Deng, T.; Seminario, J. M.; Hu, E.; Yang, X.-Q.; Balbuena, P. B.; Wang, C. Highly Reversible Aqueous Zinc Batteries enabled by Zincophilic−Zincophobic Interfacial Layers and Interrupted Hydrogen-Bond Electrolytes. *Angew. Chem., Int. Ed.* **2021**, *60* (34), 18845−18851.
(46) Yao, R.; Qian, L.; Sui, Y.; Zhao, G.; Guo, R.; Hu, S.; Liu, P.; Zhu, H.; Wang, F.; Zhi, C.; Yang, C. A Versatile Cation Additive Enabled Highly Reversible Zinc Metal Anode. *Adv. Energy Mater.* **2022**, *12* (2), 2102780.

https://doi.org/10.1021/acs.nanolett.2c00398
Nano Lett. XXXX, XXX, XXX−XXX